BAG1 promotes axonal outgrowth and regeneration *in vivo* via Raf-1 and reduction of ROCK activity

Véronique Planchamp,[1,2] Christina Bermel,[1] Lars Tönges,[1] Thomas Ostendorf,[1] Sebastian Kügler,[1,3] John C. Reed,[4] Pawel Kermer,[1,3] Mathias Bähr[1,3] and Paul Lingor[1,3]

[1]Department of Neurology, University Medicine Göttingen, Robert-Koch-Str. 40, 37075 Göttingen, [2]European Research Training Network (RTN) 'Nervous System Repair', [3]DFG-Research Center for Molecular Physiology of the Brain (CMPB), Göttingen, Germany and [4]Burnham Institute for Medical Research, La Jolla, California 92037, USA

Correspondence to: Dr Paul Lingor, Department of Neurology, University Medicine Göttingen, Germany.
E-mail: plingor@gwdg.de

Improved survival of injured neurons and the inhibition of repulsive environmental signalling are prerequisites for functional regeneration. BAG1 (Bcl-2-associated athanogene-1) is an Hsp70/Hsc70-binding protein, which has been shown to suppress apoptosis and enhance neuronal differentiation. We investigated BAG1 as a therapeutic molecule in the lesioned visual system *in vivo*. Using an adeno-associated viral vector, BAG1 (AAV.BAG1) was expressed in retinal ganglion cells (RGC) and then tested in models of optic nerve axotomy and optic nerve crush. BAG1 significantly increased RGC survival as compared to adeno-associated viral vector enhanced green fluorescent protein (AAV.EGFP) treated controls and this was independently confirmed in transgenic mice over-expressing BAG1 in neurons. The numbers and lengths of regenerating axons after optic nerve crush were also significantly increased in the AAV.BAG1 group. In pRGC cultures, BAG1-over-expression resulted in a ∼3-fold increase in neurite length and growth cone surface. Interestingly, BAG1 induced an intracellular translocation of Raf-1 and ROCK2 and ROCK activity was decreased in a Raf-1-dependent manner by BAG1-over-expression. In summary, we show that BAG1 acts in a dual role by inhibition of lesion-induced apoptosis and interaction with the inhibitory ROCK signalling cascade. BAG1 is therefore a promising molecule to be further examined as a putative therapeutic tool in neurorestorative strategies.

Keywords: BAG1; ROCK2; Raf-1 kinase; retinal ganglion cell; regeneration; apoptosis

Abbreviations: AAV = adeno-associated virus; BAG1 = Bcl-2-associated athanogene-1; d.p.a. = days post-axotomy; EGFP = enhanced green fluorescent protein; ERK = extracellular signal-regulated kinase; MAPK = mitogen-activated protein kinase; pRGC = primary retinal ganglion cell

Received December 10, 2007. Revised July 29, 2008. Accepted July 30, 2008. Advance Access publication August 29, 2008

Introduction

Adult neurons of the CNS show only limited regenerative ability after traumatic or metabolic injury, which is insufficient for restoration of functionality. This can be attributed to a diminished intrinsic growth capacity of adult neurons and lesion-induced neuronal cell death but also to growth inhibition by a non-permissive environment. Strategies to overcome regeneration failure therefore should address all of these challenges at once in order to restore functional neuronal circuits (Schwab, 2004).

Bcl-2-associated athanogene-1 (BAG1) is a multifunctional protein binding to Hsp70/Hsc70 (Takayama *et al.*, 1995; Zeiner and Gehring, 1995). Over-expression of BAG1 results in enhanced tumour cell proliferation, increased cell motility and resistance to apoptosis (Takayama *et al.*, 1995,

1999). Neurite length and generation time are significantly increased upon BAG1 transfection *in vitro* (Kermer *et al.*, 2002). Neuroprotective effects were observed in transgenic mice over-expressing BAG1 in neurons, which show a reduction in ischaemic lesion volume following middle cerebral artery occlusion (Kermer *et al.*, 2003). BAG1$^{-/-}$ mice die during embryogenesis due to failed neurogenesis, suggesting an important role for BAG1 in neuronal differentiation and neuronal survival (Gotz *et al.*, 2005).

BAG1 also interacts with and activates the Raf-1 kinase, which is an upstream element of the Ras-Raf-mitogen-activated protein kinase (MAPK)-cascade. BAG1-mediated Raf-1 activation is Ras-independent and subsequently activates the downstream extracellular signal-regulated kinase (ERK) pathway, resulting in cell growth and differentiation

(Wang *et al.*, 1996; Song *et al.*, 2001). Recently, Raf-1 has been shown to interact with ROCK2, a major component of an axonal growth inhibitory signalling pathway. Fibroblasts with conditionally ablated Raf-1 showed ROCK2 hyperactivity and mislocalization at the membrane, leading to dysregulation of the actin and vimentin cytoskeleton (Ehrenreiter *et al.*, 2005). In addition, Raf-1 was reported to physically associate with ROCK2 and to negatively regulate its activity (Piazzolla *et al.*, 2005). Within the cascade triggered by myelin-derived inhibitors of axonal growth, ROCK2 has a pivotal regulatory role in transmission of the inhibitory signal from the small GTPase RhoA to LIM kinase, which in turn regulates actin homeostasis (Schwab, 2004). Inhibition of ROCK by pharmacological inhibitors increases the number and length of regenerating retinal ganglion cells (RGC) after optic nerve crush *in vivo* and counteracts inhibitory signalling by chondroitin sulphate proteoglycans *in vitro* (Lingor *et al.*, 2007).

Here, we investigated the effects of AAV-mediated BAG1-over-expression in the lesioned RGC system *in vivo*. We show that BAG1 acts in a dual way by inhibiting lesion-induced apoptosis and enhancing axonal growth via suppression of ROCK signalling, making it a promising molecule for neurorestorative approaches in the CNS.

Material and Methods
Cloning of AAV.BAG1 and viral vector production
Subcloning of BAG1 cDNA into the AAV expression cassette was performed using the bicistronic vector pAAV-6p1, the plasmid pBAG1 (Kermer *et al.*, 2002), and the subcloning vector pBluescript II KS (Stratagene, Karlsruhe, Germany). AAV genome integrity, indispensable for the virus production, was confirmed by digestion with SmaI, which cuts within the ITR regions responsible for the proper replication of the virus. The AAV.EGFP control vector has been previously used in our group (Malik *et al.*, 2005).

Viral vectors were propagated in HEK 293 cells using the pDG helper (Grimm *et al.*, 1998), to exclude any adenoviral contamination. Viral particles were purified according to established protocols (Zolotukhin *et al.*, 1999) by iodixanol step-gradient centrifugation. Samples were then purified and concentrated by heparin-affinity chromatography on an ÄKTA FPLC system using 1 ml HiTrap Heparin FF columns (Amersham, Buckinghamshire, United Kingdom). FPLC-purified/concentrated vectors were desalted by dialysis against PBS. Genome titres were determined by quantitative PCR and purity was confirmed by PAGE. Titre calculations are based on the assumption that vector preparations contained a ratio of a 1:30 transducing units versus viral particles. Due to the neuron-specific expression characteristics of the synapsin promoter (Kugler *et al.*, 2001), functional titres of the vectors were confirmed by EGFP expression analysis in cultured primary rat hippocampal neurons. Lysates obtained from these neuronal cultures were used to confirm protein expression from the viral vectors by immunoblotting.

Primary retinal ganglion cell culture
For immunopurified rat RGC culture, Wistar rat pups were sacrificed on postnatal Days 7–8. RGCs were purified according

to a two-step panning protocol for Thy-1 to >99.5% purity described previously (Barres *et al.*, 1988). Cells were plated at a density of 7000 per well on 24-well plates (Sarstedt, Nümbrecht, Germany) containing coverslips coated with poly-D-lysine and laminin and cultured in serum-free neurobasal medium (Gibco, Karlsruhe, Germany), supplemented with glutamine, cysteine, pyruvate, triiodothyronine, B-27 supplement, BSA, transferrin, progesterone, putrescine, sodium selenite (all Gibco), forskolin 10 μM, human BDNF (Tebu, Offenbach, Germany) 50 ng/ml, insulin (Sigma, Taufkirchen, Germany) 5 μg/ml and CNTF (Tebu) 10 ng/ml. 1.5×10^8 i.u. of viral vectors were applied one day after plating in 250 μl medium. Medium was refilled to 500 μl the following day. For Raf-1 kinase inhibition studies, 500 nM Raf-1 kinase inhibitor I in solution (Calbiochem, La Jolla, CA, USA) or DMSO (AppliChem, Darmstadt, Germany) was added to the medium 1 day after virus application and kept for the culture duration (incubation time 3 days). Application was renewed after 2 days.

Quantification of primary RGCs (pRGCs) neurite length
pRGCs expressing the EGFP reporter gene (Day 5 after virus application) were incubated in a climate chamber for live cell imaging (37°C, 5% CO_2) on a fluorescence inverted microscope (Axiovert, Zeiss, Oberkochen, Germany) equipped with a CCD camera and AxioVision software (Zeiss). Contrast phase photographs of two random visual fields per culture well were taken with a 10× objective and neurite length was evaluated semi-automatically using the axon tracing module of 'Image J' (Free Java software provided by the National Institutes of Health, Bethesda, Maryland, USA). Total neurite length was divided by cell number and expressed as averaged neurite length. Experiments were performed at least in triplicate.

Quantification of pRGCs growth cone surface, cytosolic Raf-1 and perinuclear ROCK2 stainings
For evaluation of RGC growth cone surface, photomicrographs of cells stained with anti-phospho-ADF-cofilin antibody [kind gift of Dr Bamburg (Meberg and Bamburg, 2000)] were taken with a 63× oil immersion objective (Zeiss) using a fluorescence microscope (Axiovert, Zeiss) equipped with a CCD camera and AxioVision software (Zeiss). Growth cone surface, defined as the area protruding from the elongating axon, was measured and quantified using 'Image J' (National Institutes of Health).

To quantify fluorescence stainings, photomicrographs of cells stained with anti-Raf-1 or anti-ROCK2 antibodies were taken with the same settings (Cy3-filter, exposure time 500 ms; Cy5-filter, exposure time 10 s; DAPI-filter, exposure time 500 ms). For quantification of cytosolic Raf-1, an area of similar surface and shape was chosen in the middle of cytosol (see supplementary Fig. S5.A). Fluorescence was quantified using 'Image J' software (National Institutes of Health). For quantification of perinuclear ROCK2 staining, two areas of similar surface and shape were chosen at the perinuclear region and at the membrane directly opposite to the nucleus (see supplementary Fig. S5.B, C). Fluorescence was quantified using 'Image J' software (National Institutes of Health). To minimize fluorescence variability between samples, perinuclear staining data were normalized against the membrane data. Results are expressed as ratio of perinuclear/membrane fluorescence.

CSM culture

Wild-type CSM cells and CSM cells stably transfected with mouse Flag-BAG1 were previously described (Kermer *et al.*, 2002). Cultures were maintained in Dulbecco's modified Eagle's medium (PAA, Coelbe, Germany) supplemented with 10% fetal bovine serum (PAA), 1 mM L-glutamine, 100 U of penicillin/ml, 100 µg of streptomycin sulfate/ml and additional pyromycin (Sigma-Aldrich, Munich, Germany) for selection of stably transfected cells, at either 32°C (permissive temperature) or 39°C (non-permissive temperature) for 1 week (Kermer *et al.*, 2002). For lysates, CSM wild-type and BAG1 cells were plated at a density of 2.3×10^5 and 7.4×10^5 per dish (Ø 10 cm), respectively, to achieve equal densities at switch to permissive temperature. For immunofluorescence analysis, wild-type and stably transfected CSM cells were seeded on glass cover slips (Ø 10 mm) in 24-well plates at a density of 38 000 cells/well. Cultures were maintained at 32°C (non-differentiating conditions) or 39°C (differentiating conditions) in 5% CO_2 and 95% humidity. One day before fixation, cells were trypsinized and re-plated at a density of 1 : 3 and 1 : 1 respectively to allow single-cell visualization. For Raf-1 kinase inhibition studies, cells were incubated for 24 h before lysis with 500, 1000 or 2000 nM Raf-1 kinase inhibitor I in solution (Calbiochem) or DMSO (AppliChem), respectively.

Subcellular fractionations

Subcellular fractionations from CSM cells were performed using ProteoExtract® Subcellular Proteome Extraction Kit (Merck Biosciences, Darmstadt, Germany) according to the manufacturer's instructions. Protein expression was further analysed by immunoblotting.

Immunoblot analysis

The protein content of the samples was determined using the bicinchoninic acid assay (Pierce, Rockford, IL, USA) and equal amounts of protein were loaded in each lane for a sodium dodecyl sulphate–polyacrylamide gel electrophoresis (SDS–PAGE). Proteins were usually separated on a 10% stacking gel and proteins transferred to a nitrocellulose membrane (AppliChem). Membranes were blocked with 5% milk (Roth, Karlsruhe, Germany) in Tris–buffered saline/Tween-20 (TBS-T) for 1 h at RT and then incubated with primary antibodies (rabbit anti-BAG1, #1680 (Takayama *et al.*, 1995), 1 : 1000; mouse anti-Raf-1, E-10, 1 : 500; and goat anti-ROCK2, C-20, 1 : 500, both Santa Cruz Biotechnologies, Heidelberg, Germany; mouse anti-vimentin 1 : 2000, Chemicon, Schwalbach, Germany; rabbit anti-calnexin 1 : 1500, GeneTex, San Antonio, TX, USA; goat anti-calpain 1 (N-19) 1 : 500, Santa Cruz Biotechnologies, Heidelberg, Germany; mouse anti-Flag-M2 1 : 1000, Stratagene, Heidelberg, Germany; rabbit anti-phospho-c-Raf (Ser338) 1 : 500; rabbit p44/42 MAPK 1 : 1000; rabbit phospho-p44/42 MAPK (Thr202/Tyr204) 1 : 1000; mouse anti-phospho-SAPK/JNK (Thr183/Tyr185) (G9), 1 : 1000; rabbit anti-c-Jun 1 : 1500; all Cell Signalling, Frankfurt, Germany) overnight at 4°C unless stated otherwise. After 3×15 min washing in TBS-T, membranes were incubated with the appropriate HRP-coupled secondary antibodies (1 : 1000; Dianova, Hamburg, Germany) for 1 h at RT. Chemiluminescence from ECL-Plus reagents (Amersham, Arlington Heights, IL, USA) was visualized using a Fluor-S-Max imager (Bio-Rad, Munich, Germany) and Quantity One software (version 4.2.1). Protein quantification of immunoblots was performed using Quantity One software (version 4.2.1).

ROCK activity assay

ROCK activity was measured with Cyclex ROCK Kinase Activity Assay (MoBiTec, Göttingen, Germany) according to the manufacturer's instructions using 0.25 µg protein. The absorbance was measured at 450 nm using an Elisa Reader (TECAN, Crailsheim, Germany).

Immunocytochemistry

Cells grown on coverslips were first fixed in PFA 4% 10 min at room temperature (RT, 22°C), permeabilized with 100% ice-cold acetone (AppliChem) 10 min at −20°C, washed twice with PBS and blocked with 10% normal goat serum 10 min at RT. Probes were incubated with the primary antibodies [goat anti-ROCK2 1 : 50; mouse anti-Raf-1 (E-10), 1 : 50, both Santa Cruz Biotechnologies; anti-phospho-ADF-cofilin (Meberg and Bamburg, 2000)], [rabbit anti-BAG1 1 : 500, #1680 (Takayama *et al.*, 1995)] overnight at 4°C. Following $2\times$ PBS washes, appropriate Cy3- and Cy5-labelled secondary antibodies (1 : 250, Dianova) and rhodamine-conjugated phalloidin (1 : 500, Molecular Probes, Karlsruhe, Germany) were applied for 45 min at 37°C. Cells were then nuclear counter-stained with DAPI (4,6-diamidino-2-phenylindole) (Sigma) and mounted in Mowiol (Hoechst, Frankfurt, Germany). Fluorescence was observed and recorded on a Zeiss Axioplan 2 fluorescence microscope equipped with a CCD camera, an Apotome™ device and AxioVision software (Zeiss) or a Leica SP2 confocal laser scanning microscope equipped with an acousto-optical beam splitter. Fluorescence was quantified using 'Image J' software (National Institutes of Health) on pictures taken with the same settings, as indicated in text.

In vivo experiments

All animal experiments were carried out according to the regulations of the local animal research council and legislation of the State of Lower Saxony (Braunschweig). Female Wistar rats were purchased from Charles River (200–250 g; Sulzfeld, Germany). Transgenic BAG1 mice and wild-type littermates (FVB/n, Taconic Inc., Germantown, NY) were described previously (Kermer *et al.*, 2002).

Virus injection

Injections were performed intravitreally either upon brief anaesthesia by diethyl ether inhalation 3 weeks before operation or under general anaesthesia (chloral hydrate, 420 mg/kg body weight, intraperitoneally) at the time of surgery. Each injection consisted of ~3 µl containing ~2.5×10^7 i.u./µl. Care was taken to avoid any damage of the lens.

Anaesthesia and surgical approach

The anaesthesia was carried out by intraperitoneal injection of chloral hydrate (420 mg per kg body weight). A similar surgical approach was used in all three experimental paradigms to access the optic nerve. The skin was incised close to the superior orbital rim and the orbita was opened leaving the supraorbital vein intact. The intraorbital glands were partially sectioned and the superior extraocular muscles were spread by means of a small retractor. The optical nerve was exposed by longitudinal incision of the eye retractor muscle and the optic nerve sheath. After surgery retinal blood supply was verified by fundoscopy and animals with persistent retinal ischemia were excluded from the study.

Optic nerve axotomy

Axotomy of the optic nerve was performed essentially as described previously (Lingor *et al.*, 2005; Lingor *et al.*, 2008). The optic nerve was transected at a distance of ~2 mm from the posterior pole of the eye without damaging retinal blood supply. For retrograde labelling of RGCs, a 2 mm × 2 mm piece of gel foam (Braun, Melsungen, Germany) was soaked in FluoroGold (FG) (Hydroxystilbamidine; Bio-Trend, Cologne, Germany) and placed on the optic nerve stump. On Day 14 or 28 post-axotomy, animals were sacrificed by CO_2 inhalation and the eyes were extracted. The cornea, the lens and the vitreous body were removed, and the remaining eye cup containing the retina was fixed in 4% PFA in PBS pH 7.4 (PFA) for 1 h. Retinas were then extracted and flat-mounted on object-slides in glycerol-PBS (1:1). In each retinal quadrant of the transduced and non-transduced areas, three fields of 62 500 μm^2 were counted at eccentricities of one-sixth and one half and five-sixths of the retinal radius. The number of FluoroGold-positive RGC was determined by fluorescence micro-scopy (Axioplan, Zeiss) using a commercial FG narrow-band filter set (365/420 nm). Since EGFP fluorescence from strongly labelled amacrine neurons showed some leak through into this filter at longer exposure times, only those cells displaying a round shape and punctate, perinuclear FG accumulations were counted as RGCs. RGC counts were performed independently by two different investigators according to a blinded protocol. In animals treated with AAV.BAG1 or AAV.EGFP, the vector-transduced area of the retina was identified by EGFP-expressing cells. For quantification of initial RGC numbers in control Wistar rats, wild-type and transgenic mice, animals were axotomized and RGCs were retro-gradely labelled by FluoroGold. Retinas were extracted at Day 1 after axotomy and RGCs were counted. Since RGC numbers start to decline only around Day 4 following axotomy due to apoptotic cell death (Bähr, 2000), we used the Day 1 values as an indicator for initial RGC numbers.

Axotomy groups consisted of the following animal numbers included in the final evaluation: *Rats:* sacrificed at Day 1 after axo-tomy (controls): $n = 4$. Virus application at Day 0, sacrificed 14 days after axotomy: AAV.EGFP: $n = 4$, AAV.BAG1: $n = 3$. Virus applica-tion at Day 21, sacrificed at 14 days after axotomy: AAV.EGFP: $n = 5$, AAV.BAG1: $n = 6$. Virus application at Day 21, sacrificed at 28 days after axotomy: AAV.EGFP: $n = 5$, AAV.BAG1: $n = 5$. *Mice:* sacrificed at Day 1 after axotomy (controls): wild-type $n = 5$, BAG $n = 5$. Sacrificed at Day 14 after axotomy: wild-type $n = 3$, BAG $n = 4$.

Optic nerve crush

Ligation of the optic nerve was performed using a 10-0 suture (Ethicon, Johnson-Johnson, Livingston, UK) for 30 s, resulting in a complete transection of all RGC axons. The suture was removed and the operative access closed. Rats were sacrificed on Day 28 after surgery by CO_2 inhalation and immediately perfused by transcardial injection of 250 ml PBS and 200 ml 4% PFA. The eye cup containing the retina and the adjacent optic nerve were postfixed in 4% PFA in PBS for 1 h and then dehydrated in 30% sucrose at 4°C for 24 h. After embedding the previously fixed tissues in Cryomatrix (Thermoshandon, Frankfurt, Germany), longitudinal sections (16 μm thickness) of the optic nerve were prepared using a Leica cryostat and collected on gelatine-coated glass slides. For immu-nohistochemical analysis, specimens were dehumidified at 37°C for 1 h and antigen retrieval was performed for 4 h in TBS-T (pH 9.0) at 60°C. Unspecific binding was blocked by application of 10%

normal goat serum, and anti-GAP43 antibody (Biozol, Eching, Germany) was applied in a 1:250 dilution at 4°C overnight in order to stain regenerating fibres. After two PBS washes, secondary antibody (Cy-3-labelled anti-rabbit; Dianova) was applied for 45 min at RT. The sections were then nuclear counter-stained with DAPI (4,6-diamidino-2-phenylindole, Sigma) and embedded in Mowiol (Hoechst). For evaluation of RGC axon regeneration, photomicrographs were taken using a fluorescence microscope (Axioplan, Zeiss) equipped with a CCD camera and AxioVision 3 software (Zeiss). Images of whole sections were assembled from single pictures taken with a 20× objective. The number of regenerating axons at designated distances from the crush was evaluated using a counting grid superimposed on the photomicro-graph. Optic nerve crush groups consisted of the following animal numbers: Day 0: AAV.EGFP: $n = 4$, AAV.BAG1: $n = 4$. d-21: AAV.EGFP: $n = 4$, AAV.BAG1: $n = 4$.

For analysis of macrophage infiltration, unspecific binding was blocked by application of Dako Diluent (Dako, Hamburg, Germany), and mouse anti-rat CD68 (ED1) 1:200 (ABD-Serotec, Düsseldorf, Germany) was applied at 4°C overnight followed by a secondary Cy-3-labelled anti-mouse antibody. For evaluation of macrophage infiltration, ED1 (CD68)-positive cells were counted in four retinal slides per animal using a 20× objective (Zeiss).

Statistics

All *in vitro* experiments were reproduced at least in triplicate. Animal groups were as indicated in the according methods section. Differences between groups were considered statistically significant according to a one-way ANOVA followed by a parametric multiple comparison test (Dunnett test). Significances were indicated with $^*P < 0.05$, $^{**}P < 0.01$, $^{***}P < 0.001$, unless otherwise stated.

Results

Over-expression of BAG1 in RGC by bicistronic AAV-2 vectors

The cDNA of mouse Flag-p29BAG1 was first subcloned into a bicistronic recombinant AAV-2 vector, which expressed BAG1 and, in a separate expression cassette, enhanced green fluorescent protein (EGFP) (AAV.BAG1; Fig. 1A). As control construct, we used an AAV vector that expresses EGFP containing a disabled Bcl-X_L (Bcl-X_L cDNA flanked by a transcription blocker, not transcribed) expression cassette [AAV.EGFP; Fig. 1A (Malik *et al.*, 2005)].

AAV.BAG1 infection induced a concentration-dependent expression of the EGFP reporter gene in cultured hippo-campal (HC) neurons (Fig. 1B) and this was confirmed by immunoblot analysis of primary HC neuron lysates (Fig. 1C). The expression of endogenous BAG1 (Fig. 1C, upper panel, lower band) is visible in both control and infected cultures at similar levels, serving as protein loading control. Expression of the Flag-BAG1 construct was additionally verified by anti-Flag-M2 antibody.

RGC survival after axotomy is increased by BAG1

The effects of BAG1 on apoptosis and regeneration were then tested in the models of optic nerve transection (axotomy)
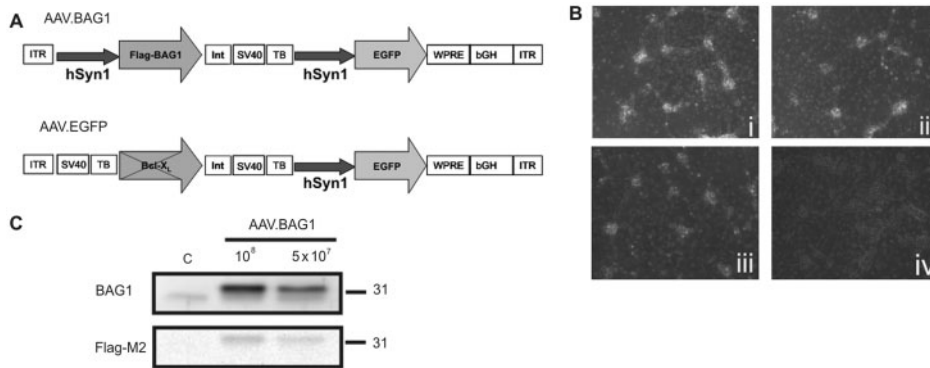
Fig. 1 Viral vectors and experimental setup. (**A**). Schematic depiction of the AAV-2 vector genomes. ITR: AAV-2 inverted terminal repeat; hSynI: human synapsin I gene promoter; Flag-BAG1: mouse BAG1 cDNA N-terminally tagged with the Flag epitope; Bcl-X_L: rat Bcl-X_L cDNA (flanked by a transcription blocker, not transcribed); Int: intron; SV40: SV40 polyadenylation site; TB: synthetic transcription blocker; WPRE: woodchuck hepatitis virus posttranscriptional regulatory element; bGH: bovine growth hormone polyadenylation site. (**B**). Titration of AAV.BAG1 in vitro. Application of 1×10^8 (i), 5×10^7 (ii) and 1×10^7 (iii) i.u. AAV.BAG1 respectively induces the expression of EGFP reporter gene in a concentration-dependent manner in primary hippocampal neurons. Non-treated control (iv). (**C**). Analysis of transgene expression by immuno blot. Application of 1×10^8 and 5×10^7 i.u. AAV.BAG1 on primary hippocampal neuron cultures induces the expression of BAG1 in a concentration-dependent manner. Endogenous expression of BAG1 (lower band), visible in control and infected cultures, was used as loading control. Expression of the Flag-BAG1 construct was additionally verified by anti-Flag-M2 antibody. Size standards in kDa are shown on the right.

and optic nerve crush in vivo. For axotomy, the virus was applied either 21 days prior to surgery (Day 21) to allow for sufficient protein expression prior to lesion or directly following axotomy (Day 0) to mimic a possible therapeutic application. Animals were sacrificed 14 or 28 days after axotomy. RGC were retrogradely labelled by administration of FluoroGold following axotomy and surviving RGC were quantified in retinal flat-mounts. Intravitreal application of 5×10^7 i.u. AAV.BAG1 or AAV.EGFP resulted in an infection of ~1/3 of the retinal area around the injection site (Fig. 2A). No cytotoxic effects were observed following virus application (Fig. 2A, ii–iv). RGC survival was evaluated by comparing RGC numbers in transfected and non-transfected areas of the same retinas. Non-transfected and AAV.EGFP-transfected areas did not significantly differ from PBS-treated controls (Fig. 2B and data not shown). When AAV.BAG1 was injected at the day of axotomy, only an insignificant trend toward increased RGC survival was observed. In contrast, virus application 3 weeks prior to axotomy resulted in a significant increase in surviving RGC (1547 ± 94 RGC/mm^2; 83.5% of control retina) compared to AAV.EGFP-treated animals (721 ± 66 RGC/mm^2; 38.9% of control retina) at 14 days post-axotomy (d.p.a) (Fig. 2B). A protective effect was also still observed 28 days after axotomy (AAV.BAG1: 1025 ± 115 RGC/mm^2; 55.3% of control retina, AAV.EGFP: 578 ± 36 RGC/mm^2; 31.2% of control retina; Fig. 2B).

Second, we compared the results obtained by AAV infection with transgenic mice over-expressing BAG1 in neurons [Fig. 2C (Kermer et al., 2003)]. At 14 d.p.a, BAG1 transgenic mice showed a ~35% improvement in RGC survival (2838 ± 53 RGC/mm^2, 59.0% of control retina) compared to their wild-type litter-mates (1852 ± 54 RGC/mm^2, 34.9%

of control retina). Initial RGC numbers (at 1 day post-axotomy) did not significantly differ between wild-type and BAG1 transgenic mice. Thus, BAG1 protects RGC from axotomy upon over-expression either from a stable transgenic or from an AAV vector.

BAG1 increases number and length of regenerating axons after optic nerve crush

We next investigated whether BAG1 promoted axonal regeneration in the non-permissive optic nerve crush model in vivo. Animals were treated with 5×10^7 i.u. of AAV.BAG1 or AAV.EGFP 21 days prior to surgery (Day-21) or immediately post-lesion (Day 0). Animals were sacrificed on Day 28 after surgery and optic nerve sections were immuno-stained for GAP-43 to identify regenerating axons (Fig. 3A). AAV.BAG1 application at the time of surgery resulted in a significant increase in number (up to 3-fold) and length of regenerating axons past the crush site compared to animals treated with AAV.EGFP. Control animals receiving AAV.EGFP showed only minor regeneration past the lesion site, while axons regenerating up to 800 μm past the crush site were only observed in animals treated with AAV.BAG1 (Fig. 3B). AAV.BAG1 application 3 weeks before injury similarly resulted in a significant increase in the number of regenerating axons. Most remarkably, an increased number of regenerating axons was observed at distances between 1000 and 2000 μm from the crush site, which were not present in the other treatment groups (Fig. 3C). To exclude effects mediated by macrophage infiltration, retinal sections were stained for ED1. No significant differences in ED1-positive cell numbers were observed between AAV.EGFP-, AAV.BAG1 and PBS-treated retinas (supplementary Fig. S1).
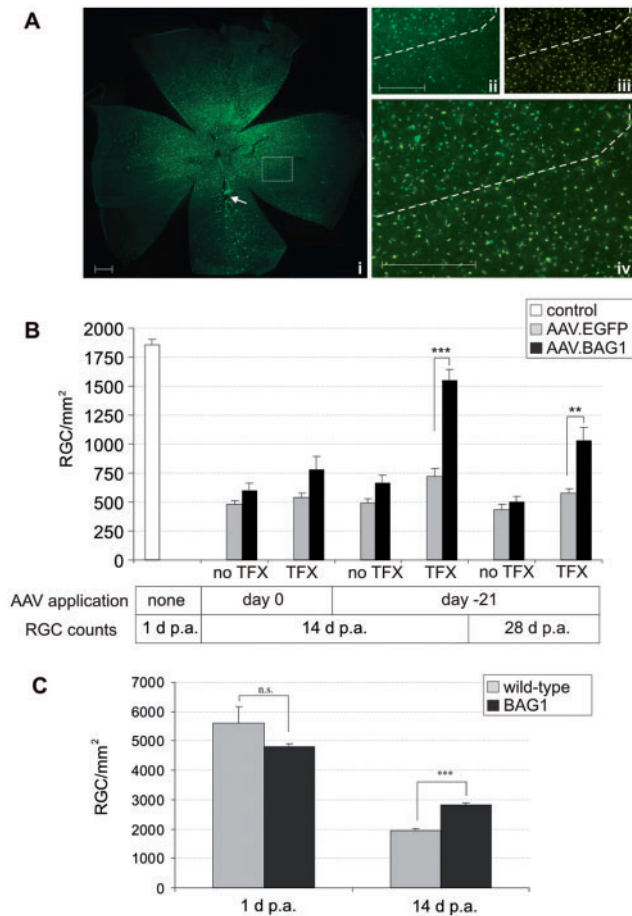
Fig. 2 RGC survival after axotomy. (**A**). (i) EGFP expression in RGCs (retinal flat mount) after intravitreal injection of 5×10^7 transducing units of AAV.EGFP 28 days following axotomy. Approximately 1/3 of the retina is transduced around the injection site (arrow). (ii–iv) Comparison of transfected and non-transfected areas (dashed line) shows that virus application does not result in cytotoxicity (ii, EGFP; iii, Fluorogold; iv, merge). Scale bar: 1 mm. Scale bar in inserts: 500 μm. (**B**). Surviving RGCs at 1 (control), 14 and 28 days post-axotomy (d. p.a.) in AAV.BAG1- or AAV.EGFP-injected rats. Bars represent means ± SEM. **$P < 0.01$, ***$P < 0.001$. TFX, transfected area; no TFX, not transfected area. (**C**). Surviving RGCs in BAG1 transgenic and wild-type mice at 1 (control) and 14 d. p.a. Bars represent means ± SEM. n.s., not significant; ***$P < 0.001$.

Neurite length and growth cone surface *in vitro* are increased by BAG1

For *in vitro* analysis of neurite length and growth cone surface, primary RGC (pRGC) cultures were infected with AAV.EGFP and AAV.BAG1 vectors. Morphological analysis was performed 5 days after vector application, when pRGC showed sufficient BAG1 and EGFP expression (supplementary Fig. S2).

Consistent with our *in vivo* data, applying AAV.BAG1 (1.5×10^8 i.u.) to pRGC resulted in increased neurite outgrowth (Fig. 4A and B). AAV.BAG1-treated pRGC showed a ~3-fold longer average neurite length (651 ± 160 μm)

compared to AAV.EGFP-treated (216 ± 58 μm) and non-treated control cells (212 ± 37 μm) (Fig. 4B). In addition, AAV.BAG1-treated pRGC had significantly larger growth cones and an increased number of filopodia (Fig. 4C). Quantitative analysis of the growth cone area showed a ~2.5-fold larger average growth cone surface (27.39 ± 3.81 μm^2) compared to AAV.EGFP-treated (10.07 ± 1.07 μm^2) and non-treated control cells (13.37 ± 2.12 μm^2) (Fig. 4D). The number of filopodia per growth cone exhibited a similar increase, with an average of 3.9 ± 0.4 filopodia per growth cone compared to 1.5 ± 0.3 and 0.8 ± 0.4 in AAV.EGFP-treated and non-treated control cells, respectively (Fig. 4E).

Translocation of Raf-1 and ROCK2 in primary RGC after BAG1-over-expression

Our *in vivo* data suggested neuroprotective and regeneration-promoting roles for BAG1 in lesioned RGC, but the underlying molecular mechanisms remained unclear. BAG1 has previously been shown to activate Raf-1 kinase (Wang *et al.*, 1996). The lack of Raf-1 has been demonstrated to result in the recruitment of ROCK2 to the cell membrane and ROCK2 hyperactivity (Ehrenreiter *et al.*, 2005). We thus investigated whether Raf-1-induced translocation of ROCK2 could be involved in BAG1-mediated effects on regeneration.

We examined the subcellular localization of Raf-1 and ROCK2 upon BAG1-over-expression. Pseudo-confocal fluorescence microscopy of non-treated and AAV.EGFP-treated pRGC showed membrane-bound localization of both Raf-1 and ROCK2 (Fig. 4F and data not shown). In contrast, AAV.BAG1 induced more cytoplasmic expression of Raf-1 (Fig. 4G). In both AAV.EGFP and AAV.BAG1-treated pRGC, phospho-cofilin was mostly localized at the cell membrane (Fig. 4F and G). ROCK2 partially colocalized with phospho-cofilin in control pRGC. In contrast, AAV.BAG1-treated cells showed a strong perinuclear concentration of ROCK2 compared to AAV.EGFP-treated cells. Consistent with a previous report (Ehrenreiter *et al.*, 2005), we observed a colocalization of Raf-1 and ROCK2, which was most pronounced at the membrane (Fig. 4F and G). Quantification of fluorescence showed a significant increase of cytoplasmic Raf-1 (~2-fold) and perinuclear ROCK2 (~3-fold) in AAV.BAG1-treated cells compared to controls (9.21 ± 0.76 arbitrary fluorescence units vs 4.88 ± 0.46 arbitrary fluorescence units, and 2.67 ± 0.23 arbitrary fluorescence units vs 0.74 ± 0.07 arbitrary fluorescence unit, respectively; Fig. 4H and I).

BAG1 induces Raf-1 and ROCK2 translocation in CSM cells

To further examine the subcellular protein localization of Raf-1 and ROCK, we used the rat CSM14.1 neuronal cell line stably transfected with Flag-BAG1 (Kermer *et al.*, 2002). CSM14.1 cells have larger cell bodies than RGC, allowing for a better identification of cellular structures and the generation of sufficient amounts of protein lysates for subcellular
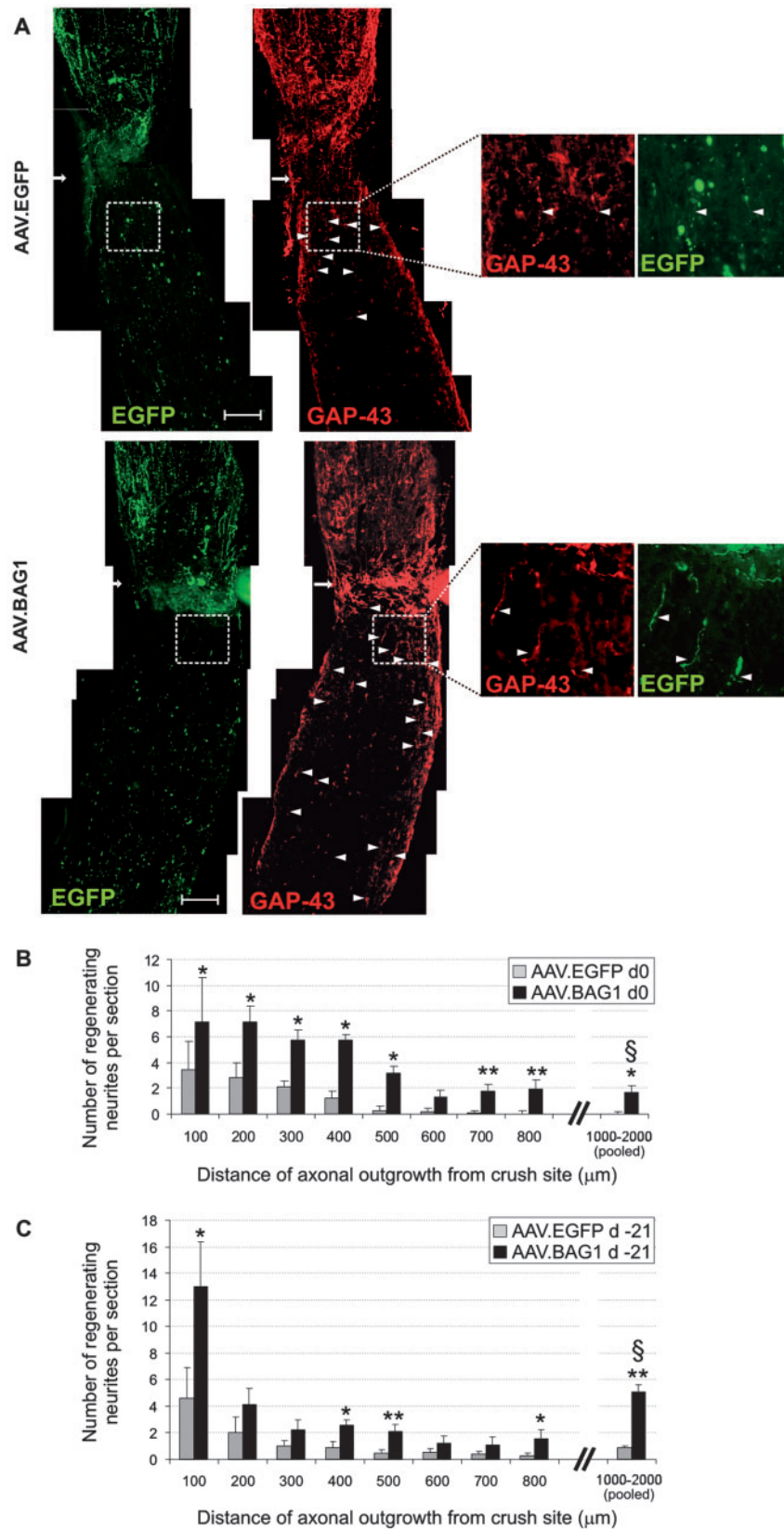
Fig. 3 Axonal regeneration after optic nerve crush. (**A**). Representative photomicrographs of regenerating axons in optic nerve sections of animals treated with 5×10^7 i.u. AAV.EGFP and AAV.BAG1 respectively 21 days before lesion. GAP43 positive regenerating axons (indicated by arrow heads) extend beyond the crush site (arrows). Scale bar: 200 μm. **B and C**. Number of regenerating axons 28 days after optic nerve crush at designated distances from the crush site when AAV-2 vectors were applied at the day of surgery (**B**) or 21 days before surgery (**C**). Numbers of regenerating axons between 1000 and 2000 μm from the crush were pooled for better readability. Bars represent means ± SEM. *$P < 0.05$, **$P < 0.01$. § $P < 0.05$ between groups in **B** and **C**.
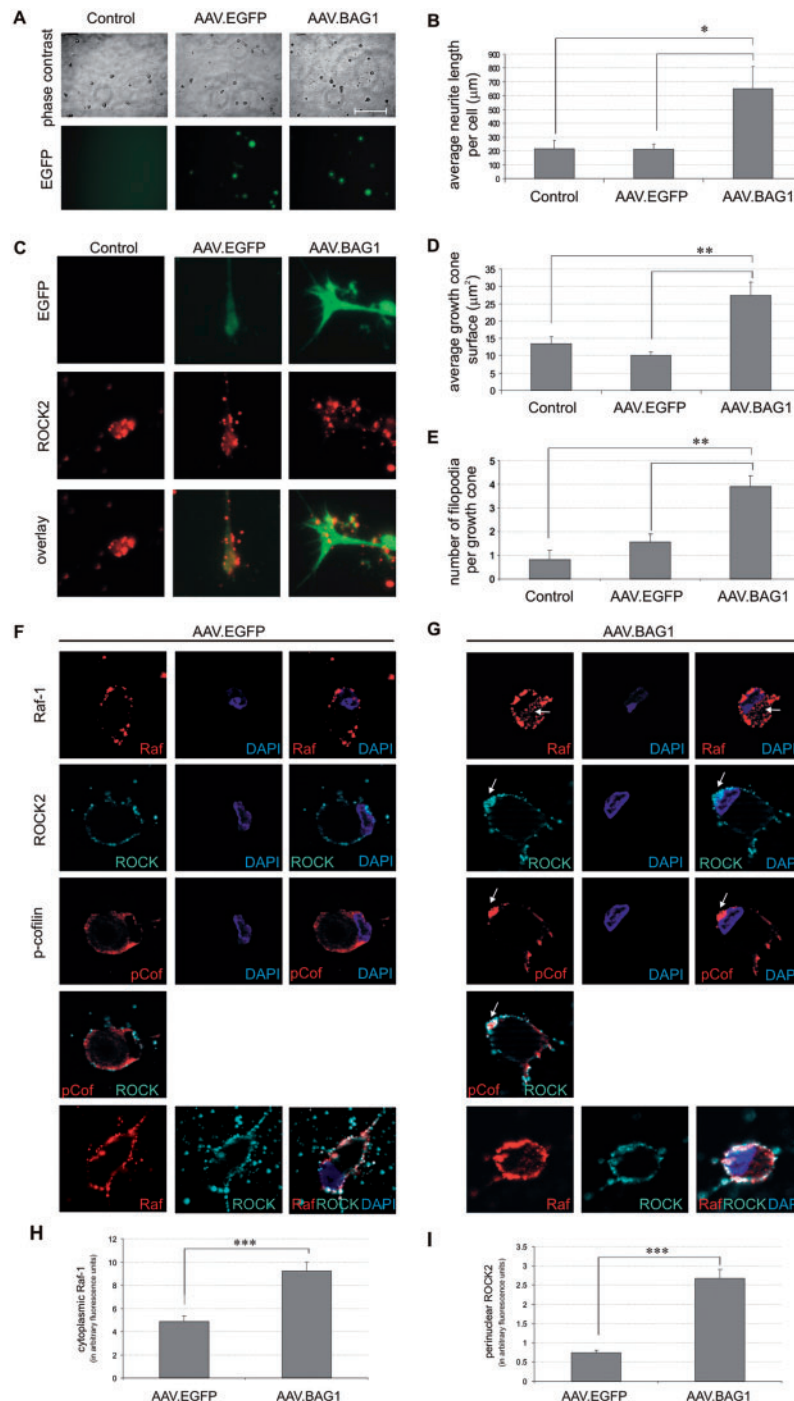
Fig. 4 BAGI induces translocation of Raf-1 and ROCK2 in primary RGCs. (**A**). Representative micrographs (phase contrast, upper panel; EGFP, lower panel) of untreated (control), AAV.EGFP- and AAV.BAGI-treated pRGCs. Scale bar: 200 μm. (**B**). Quantitative analysis of neurite outgrowth at 5 days after virus application. Application of AAV.BAGI resulted in a significant increase in neurite outgrowth compared to AAV.EGFP and non-treated cells. Bars represent means ± SEM. For all treatments, $n = 4$. *$P < 0.05$. (**C**). Representative micrographs of growth cones in pRGCs treated with AAV.BAGI, AAV.EGFP or untreated controls. Growth cones are visualized by EGFP expression and ROCK2 immunocytochemistry. (**D**). Quantitative analysis of growth cone surface at 5 days after virus application. Bars represent means ± SEM. Control, $n = 36$; AAV.EGFP, $n = 33$; AAV.BAGI, $n = 29$. **$P < 0.01$. (**E**). Quantitative analysis of number of filopodia per growth cone at 5 days after virus application. Bars represent means ± SEM. Control, $n = 27$; AAV.EGFP, $n = 33$; AAV.BAGI, $n = 31$. **$P < 0.01$. **F and G**. Photomicrographs depicting Raf-1, ROCK2 and phospho-cofilin subcellular localization in pRGCs. Cells were treated with AAV.EGFP (**F**) and AAV.BAGI (**G**) respectively for 5 days and stained with antibodies specific for Raf-1, ROCK2 and phospho-cofilin followed by the appropriate fluorochrome-conjugated antibodies and DAPI. Arrows indicate translocation of Raf-1 to the cytoplasmic compartment (upper row) and translocation of ROCK2 to the nuclear/perinuclear space (rows 2–4) in AAV.BAGI-treated cells as compared to AAV.EGFP treated controls. Raf-1 and ROCK2 partially colocalize (row 5). (**H**). Quantitative analysis of cytoplasmic Raf-1 expression. Data are expressed in arbitrary fluorescence units. AAV.EGFP, $n = 21$; AAV.BAGI, $n = 29$. ***$P < 0.001$. (**I**). Quantitative analysis of nuclear ROCK2 expression. Data are expressed in arbitrary fluorescence units. AAV.EGFP, $n = 22$; AAV.BAGI, $n = 28$. ***$P < 0.001$.
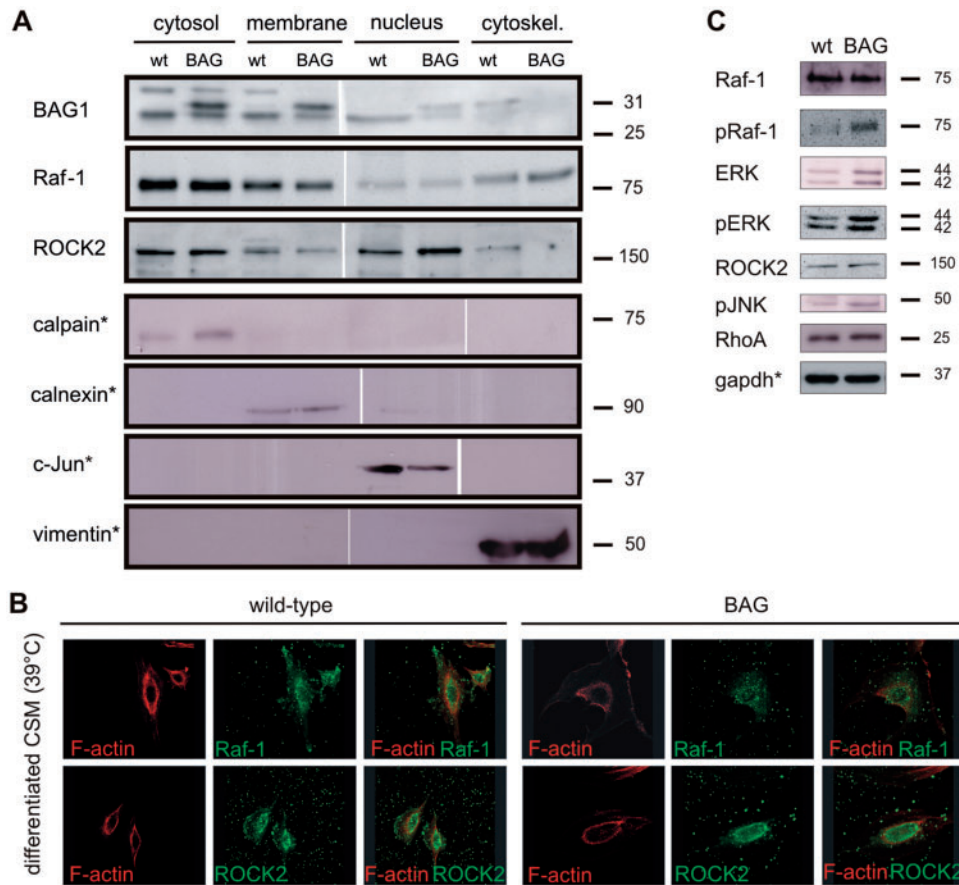
Fig. 5 Subcellular localization of Raf-1 and ROCK2 in BAGI-over-expressing CSM cells. (**A**). Immuno blot analysis of subcellular expression of BAGI, Raf-1, and ROCK2 in differentiated CSM cells respectively. Endogenous expression of BAGI (lower band) was used as a loading control. Calpain, calnexin, c-Jun and vimentin (*, representative immuno-blots) were probed as markers of fraction specificity. Experiments were repeated at least three times with cells from different passages. Size standards in kDa are shown on the right. For immunoblot quantification, see supplementary Figure S4B and D. (**B**). Cellular localization of Raf-1 and ROCK2 in differentiated wild-type and BAGI-over-expressing CSM cells. Cells stained with rhodamine-conjugated phalloidin and antibodies specific for Raf-1 and ROCK2 followed by the appropriate fluorochrome-conjugated antibodies were analysed by confocal microscopy. (**C**). Immunoblot analysis of downstream effectors of the Ras-Raf-MAPK cascade and RhoA in differentiated CSM cells. Gapdh (*representative picture) was probed for each immuno-blot as a loading control. Experiments were repeated at least three times with cells from different passages. Size standards in kDa are shown on the right. For immuno-blot quantification, see supplementary Figure S4F. wt, wild-type CSM cells; BAG, BAGI-over-expressing CSM cells.

fractionation studies. Upon growth at permissive temperature (32°C), CSM cells remain in a non-differentiated state and proliferate. Incubation at non-permissive temperature (39°C) results in their differentiation into neurons. Culture lysates from wild-type or BAG1 over-expressing CSM cells were analysed by immunoblotting using antibodies directed against BAG1, Raf-1, and ROCK2.

BAG1 expression in differentiated cells remained more cytosolic when compared to membrane expression (Fig. 5A) while it was slightly stronger in the nucleus in non-differentiated cells (supplementary Fig. S3A). These results are in line with previous reports of a shift from nuclear to cytosolic localization of BAG1 upon differentiation (Song et al., 2001). Raf-1 expression levels in cytosol, membrane and nucleus did not significantly differ between wild-type and BAG1-over-expressing cells and were independent of differentiation state. However, in the cytoskeletal fraction,

non-differentiated wild-type cells show significantly higher Raf-1 protein level than differentiated BAG1-over-expressing cells (Fig. 5A, S3A and S4A, B). This suggests a shift of Raf-1 to the cytoskeleton in differentiated cells upon BAG1-over-expression, which confirms our results obtained in pRGC cultures (Fig. 4E, F, H, I). A similar effect was observed in CSM cells immunostained for Raf-1 (Fig. 5B). Immuno-blot analysis of ROCK2 showed significantly higher expression levels in the nuclear fraction upon BAG1-over-expression in both differentiated and non-differentiated cells (Fig. 5A, S3A and S4C, D). In accordance with the results obtained in pRGC, ROCK2 expression shifted to the perinuclear and nuclear regions in differentiated BAG1-over-expressing CSM cells (Fig. 5A).

To exclude changes in overall expression, we analysed protein expression in whole cell lysates. Figure 5C shows the expression levels of Raf-1, phospho-Raf-1, the downstream

effectors of the Ras-Raf-pathway ERK, phospho-ERK and phospho-JNK as well as RhoA and ROCK2 in differentiated CSM cells. BAG1-over-expression induced a significant increase in phospho-Raf-1, while Raf-1 levels remained stable. These results are in line with previous works reporting Raf-1 activation (indicated by phosphorylation) by BAG1 (Wang *et al.*, 1996; Song *et al.*, 2001). ERK and phospho-ERK levels were also increased in BAG1-over-expressing cells (Kermer *et al.*, 2002). Levels of phospho-JNK show a moderate increase upon BAG1-over-expression. No significant differences were observed in RhoA and ROCK2 expression levels between differentiated wild-type and BAG1-over-expressing cells.

ROCK activity is decreased in a Raf-1-dependent manner upon BAG1-over-expression

Lack of Raf-1 has been previously demonstrated to result in the recruitment of ROCK2 to the cell membrane and an increase of ROCK activity (Ehrenreiter *et al.*, 2005). Accordingly, our *in vitro* results showed that over-expression of BAG1 induced a differential translocation of Raf-1 and ROCK2. We now wanted to know whether over-expression of BAG1 can influence ROCK activity in addition to its effect on protein localization. We therefore quantified ROCK activity by ELISA in whole lysates of BAG1-over-expressing or wild-type CSM cells. ROCK activity of non-differentiated cells did not significantly differ between BAG1-over-expressing cells and wild-type controls. In contrast, over-expression of BAG1 in differentiated neuron-like cells significantly reduced ROCK activity by ∼50% compared to wild-type cells (Fig. 6A).

We further examined whether Raf-1 could be the molecular link between BAG1-over-expression and the observed decrease in ROCK activity. CSM cells were treated for 24 h with the Raf-1 kinase inhibitor GW5074 or DMSO before lysis and Raf-1 inhibition was verified by immuno-blot analysis. Inhibitor application resulted in a decrease of phospho-Raf-1 and its activated downstream effector phospho-ERK compared to DMSO-treated controls, demonstrating the efficient inhibition of Raf-1. ROCK2 expression was not influenced by Raf-1 inhibition (Fig. 6B).

ROCK activity was then quantified in lysates of cells treated with the Raf-1 kinase inhibitor. Application of GW5074 resulted in a concentration-dependent increase in ROCK activity, both in wild-type and BAG1-over-expressing CSM cells (Fig. 6C). Specifically, incubation with 2000 nM GW5074 significantly increased ROCK activity, resulting in a significantly higher enzymatic activity in wild-type and BAG1-over-expressing CSM cells compared to DMSO controls ($138.5 \pm 8.6\%$ vs $100.0 \pm 4.3\%$ and $88.3 \pm 6.2\%$ vs $66.3 \pm 5.9\%$, respectively).

To confirm that Raf-1 is the molecular link between BAG1-over-expression, decrease in ROCK activity, and enhanced neurite outgrowth, we tested whether application

of GW5074 had an impact on the neurite outgrowth of pRGC. Upon DMSO treatment, AAV.BAG1-treated cells exhibit a ∼3-fold higher average neurite length compared to AAV.EGFP ($942.4 \pm 74.6\,\mu m$ and $314.8 \pm 0.4\,\mu m$ respectively, Fig. 6D). In contrast, application of 500 nM GW5074 dramatically impaired neurite outgrowth (AAV.BAG1: $411.1 \pm 32.6\,\mu m$; AAV.EGFP: $337.6 \pm 70.2\,\mu m$). Analysis by pseudo-confocal fluorescence microscopy of co-staining with Raf-1 and ROCK2 showed that following GW5074 application, AAV.BAG1-treated cells exhibit a pattern of Raf-1 and ROCK2 membrane localization similar to AAV.EGFP-treated and non-AAV-treated controls (Figs. 6E and 4F and data not shown).

Discussion

Successful regenerative strategies for the CNS depend on the simultaneous targeting of different mechanisms, such as lesion-induced neuronal cell death and axonal growth inhibitory signals derived from myelin proteins. In the present study, we thus evaluated a gene therapeutic approach to counteract apoptosis and axonal growth inhibition by AAV-mediated over-expression of BAG1 in RGC.

BAG1 is neuroprotective and promotes regeneration *in vivo*

BAG1 has previously been shown to act in an anti-apoptotic and neuroprotective manner in an experimental stroke model *in vivo* (Kermer *et al.*, 2003). To assess neuroprotection after traumatic injury we used the optic nerve axotomy model, in which ∼80–90% of RGC degenerate 2 weeks following deafferentiation (Kermer *et al.*, 1998; Lingor *et al.*, 2005; Malik *et al.*, 2005). The AAV vector was applied 3 weeks prior to surgery (Day 21), allowing for sufficient protein expression before lesioning, or at the time of axotomy (Day 0) mimicking a possible therapeutic application. Although sufficient retinal transgene expression was observed in both groups at the time of extraction of the retinas (Day 14), only the group receiving AAV.BAG1 injection prior to the lesion showed a significant increase (∼70%) in surviving RGC numbers compared to AAV.EGFP controls (Fig. 2B). The neuroprotective effect of AAV.BAG1 was also still present at 28 days after axotomy (Fig. 2B). This is in line with previous reports demonstrating AAV-mediated neuroprotection of RGCs up to 8 weeks after axotomy (Malik *et al.*, 2005). AAV-mediated transgene expression under the human synapsin promoter requires several days to be fully expressed in infected neurons (Kugler *et al.*, 2003), which may therefore not be sufficient to counteract apoptosis when applied simultaneously with the lesion. The slightly higher numbers of surviving RGC observed in AAV.EGFP-infected areas, though not statistically significant, may be due to cytokine secretion following the virus application itself (Straten *et al.*, 2002). The cytoprotective effect of BAG1 was confirmed in transgenic
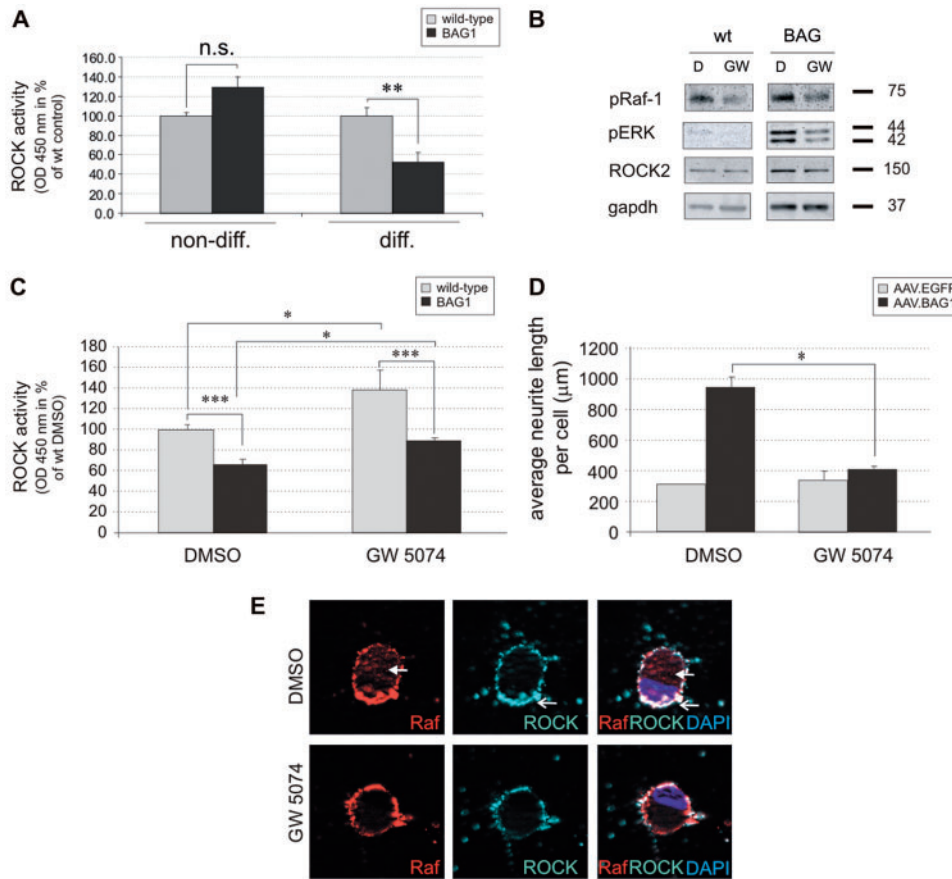
Fig. 6 Over-expression of BAG1 reduces ROCK activity in neuron-like CSM cells. (**A**). ROCK activity in wild-type and BAG1 over-expressing CSM cells. Data are from three independent experiments each. Bars represent means ± SEM., n.s. not significant; **$P<0.01$. non-diff., non-differentiated; diff., differentiated. (**B**). Immuno-blot analysis of phospho-Raf-1, phospho-ERK and ROCK2 expression following Raf-1 kinase inhibition. Application of 500 nM Raf-1 kinase inhibitor GW5074 (GW) leads to a decreased phospho-Raf-1 expression and its activated downstream effector phospho-ERK compared to DMSO-treated control (**D**). Gapdh was probed for each immuno-blot as a loading control. Experiments were repeated at least three times with cells from different passages. Size standards in kDa are shown on the right. For immuno-blot quantification, see supplementary Figure S4G. wt, wild-type; BAG, BAG1-over-expressing CSM cells. (**C**). Inhibition of Raf-1 kinase activity by GW5074 (2000 nM) affects ROCK activity. Data are from at least three independent experiments each. Bars represent means ± SEM. *$P<0.05$, ***$P<0.001$. (**D**). Neurite length in pRGC after treatment with the Raf-1 inhibitor GW5074 or DMSO (control). AAV.BAG1-transduced pRGC have longer neurites than their AAV.EGFP-treated controls and this effect of BAG1 is reversed by treatment with the Raf-1 inhibitor GW5074. For all conditions, $n=4$. (**E**). Subcellular localization of Raf-1 and ROCK2 in AAV.BAG1-treated pRGCs after application of Raf-1 inhibitor (GW5074) or DMSO (control). Cells were stained with antibodies specific for Raf-1 and ROCK2 followed by the appropriate fluorochrome-conjugated antibodies and DAPI. Arrows indicate translocation of Raf-1 to the cytoplasmic compartment and ROCK2 to the nuclear/perinuclear space only in the control condition (DMSO-treated), while GW5074 treatment reverses the BAG1-induced translocation of Raf-1 and ROCK.

BAG1 mice, which showed a ∼50% increase in RGC survival compared to wild-type littermates (Fig. 2C). The number of surviving RGCs post-axotomy in AAV.EGFP-treated rats (Fig. 2B) was lower than the corresponding numbers in wild-type mice (Fig. 2C). Interestingly, FVB/N mice–the background strain for our BAG1 transgenics–have previously been shown to be more robust following an axotomy lesion than their counterparts with a C57BL/6 background (Liu *et al.*, 2003). Thus higher surviving RGC numbers following axotomy may be due to differences in species and strain.

In addition to its neuroprotective effects, BAG1-over-expression *in vitro* results in longer neurites and increased generation time in CSM cells (Kermer *et al.*, 2002). In our

model, RGC regeneration was quantified 28 days after crush. Here, transgene expression after vector injection at the day of lesion (Day 0) was found sufficient to significantly enhance axon regeneration in AAV.BAG1-treated animals, opening a window for future therapeutic options. BAG1-over-expression resulted in an up to 3-fold higher number of regenerating axons extending 800 μm or more past the crush site compared to animals treated with AAV.EGFP, which showed a maximal regeneration length of 600 μm (Fig. 3). The increased survival observed 2 weeks after axotomy in animals treated with AAV.BAG1 may partly contribute to the better regeneration response. However, BAG1-transfected RGC were not only increased in number,

but also extended longer axons past the crush site. Most interestingly, when animals were injected with AAV.BAG1 21 days before axotomy, an increased number of regenerating neurites was found at longer distances (>1000 μm beyond the crush site) compared to animals that received the AAV injection at the day of lesion (Fig. 3C). Pre-treatment with AAV.BAG1 thus seems to more strongly disinhibit long distance axonal regeneration. Our *in vitro* data suggests that this could be attributed to an earlier onset of BAG1-induced inhibition of ROCK activity in the pre-treatment group.

In vitro, BAG1-over-expression enhances neurite outgrowth and modifies growth cone morphology by increasing growth cone area and the number of filopodia (Fig. 4). Together, these results suggest that BAG1 is not only neuroprotective, but also plays an important role in promoting regeneration by triggering cellular remodelling involved in neurite outgrowth. For functional restoration in the CNS, the simultaneous targeting of apoptosis and growth inhibition is crucial. For example, AAV-2-mediated expression of the anti-apoptotic molecule Bcl-X_L resulted in comparable RGC survival rates at 14 d.p.a (Malik *et al.*, 2005). However, Bcl-X_L expression alone failed to enhance axonal growth in retinal explants (Dietz *et al.*, 2006). AAV-mediated expression of the ciliary neurotrophic factor (CNTF) has been shown to potently increase the number of surviving RGC and to promote regeneration (Leaver *et al.*, 2006*a*). When AAV-CNTF was applied to Bcl-2 transgenic mice, an even stronger regenerative response could be observed, but the differences between wild-type and Bcl-2 transgenic mice levelled off at longer distances from the crush suggesting rather a primary effect on survival than on regenerative ability (Leaver *et al.*, 2006*b*). Latter studies clearly demonstrate that the overall regenerative outcome crucially depends on survival of axotomized neurons, but that the length of regenerating axons does not directly correlate with better survival. In contrast to this, our data demonstrates that AAV.BAG1-treated animals grew not only more, but longer axons and this effect was sustained at longer distances from the crush site (Fig. 3). The overall regeneration in the present study is less pronounced than in previous studies of our group, where substances, e.g. CNTF or ROCK inhibitors, were applied intravitreally and thus target the entire RGC population (Lingor *et al.*, 2007, 2008). In our present work, only partial transduction of the retina by AAV was intended in order to obtain intraretinal controls within the same animal, which necessarily limits the number of targeted RGCs, but at the same time permits a qualitative evaluation of the regeneration response.

CNTF and many other growth factors mainly act via inhibition of lesion-induced apoptosis and increase the intrinsic regenerative capacity of adult neurons by activation of pro-survival pathways, e.g. MAPK, Akt and STAT3 (Park *et al.*, 2004). Pathways which propagate growth inhibitory signals from myelin-derived molecules are only moderately modulated by CNTF signalling (Lingor *et al.*, 2008) and this

may account for the persistence of growth inhibition at longer regeneration distances.

Regulation of subcellular translocation of Raf-1 and ROCK2 by BAGl

BAG1 has been shown to bind to and activate the kinase Raf-1 (Wang *et al.*, 1996; Song *et al.*, 2001). In turn, Raf-1 was reported to colocalize and associate with ROCK. Lack of Raf-1 resulted in the recruitment of ROCK2 to the cell membrane and ROCK2 hyperactivity (Ehrenreiter *et al.*, 2005). Accordingly, our *in vitro* results obtained by immunocytochemistry and subcellular fractionation show that BAG1-over-expression induces Raf-1 translocation from a membrane-associated localization to the cytoplasm and ROCK2 translocation from the membrane to the perinuclear region respectively (Figs 4 and 5). Following activation, Raf-1 has been reported to undergo intracellular redistribution, to the perinuclear space (e.g. Rapp *et al.*, 1988), or into the nucleus (Olah *et al.*, 1991; Brennscheidt *et al.*, 1994). Our subcellular fractionation results are in line with a previous report showing a mostly cytoplasmic and partly perinuclear localization of Raf-1 in brain lysates (Morice *et al.*, 1999). Thus, over-expression of BAG1 triggers Raf-1 translocation, recruiting Raf-1 to a functionally different cellular compartment.

Our data also shows that ROCK2 translocates from membrane localization to the perinuclear and nuclear space upon BAG1-over-expression in pRGCs and CSM cells. ROCK2 is reported to be essentially cytosolic and to translocate to the membrane upon Rho-activation (Matsui *et al.*, 1996). In fibroblasts, ROCK2 is found mostly at the cell membrane and in the perinuclear space (Yoneda *et al.*, 2005), while recent studies also observed ROCK in the nucleus associated with Cdc25A or p300 acetyltransferase (Bhowmick *et al.*, 2003). This suggests that, while active at the membrane under physiological conditions, ROCK2 translocation to the cytosol and perinuclear space might result in enzymatic inhibition and possible yet unknown functions in regulating gene transcription. Moreover, ROCK2 partially colocalizes with ADF-cofilin, consistent with its well-described role in actin stabilization (Mueller *et al.*, 2005).

Regulation of ROCK activity by BAGl via Raf-1

Our results thus suggest that BAG1-induced regeneration is mediated by Raf-1. *In vitro*, BAG1-over-expression activates Raf-1 and its downstream effector ERK, a finding consistent with previous studies (Wang *et al.*, 1996; Song *et al.*, 2001; Kermer *et al.*, 2002; Liman *et al.*, 2005). ERK regulation of gene transcription plays a major role in developmental axon growth (Markus *et al.*, 2002). Accordingly, Raf-1 kinase inhibition reduced phospho-ERK expression in pRGC (data not shown) and impaired axon outgrowth.
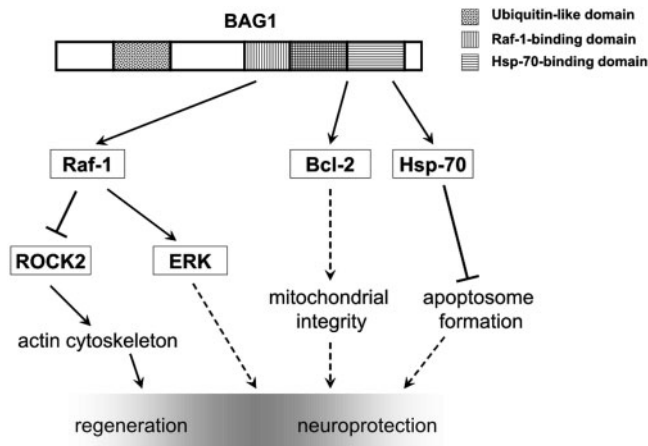
Fig. 7 BAG1 is involved in the regulation of signalling cascades in neuroprotection and regeneration. Model of BAG1-mediated regeneration and neuroprotection based on the reported findings and the current literature. BAG1 activates Raf-1, which leads to the activation of the MAPK pathway and inhibition of ROCK activity. Activation of ERK may play a role in enhancement of the intrinsic capability of neurons to regenerate by stimulating neurite outgrowth, while decrease in ROCK enzymatic activity, in addition to the translocation of ROCK2 from a membrane-bound to cytosolic and perinuclear space, may result in modulation of actin cytoskeleton and growth cones. Through its Hsp70-binding domain, BAG1 activates Bcl-2 and Hsp-70, thus enhancing survival. Full lines: direct interaction; dashed lines: indirect interaction. Pointed end: stimulation; bar end: inhibition.

Additionally, BAG1-over-expression significantly reduces ROCK activity *in vitro*, although ROCK2 expression levels remain stable within the cell. This effect does not involve RhoA, an upstream activator of ROCK, but is dependent on Raf-1 kinase. Application of Raf-1 kinase inhibitor increases ROCK activity in wild-type and BAG1-over-expressing cells, suggesting that Raf-1 is responsible for the BAG1-mediated reduction in ROCK activity in CSM cells. The N-terminal regulatory domain of Raf-1 was shown to negatively regulate the kinase domain of ROCK (Piazzolla *et al.*, 2005), while the Raf-1 kinase domain is not involved in ROCK interaction (Ehrenreiter *et al.*, 2005). This suggests that the sterical impairment in the Raf-1/ROCK interaction through inhibitor-binding results in a reduction of ROCK inhibition, even though we cannot rule out that the observed effect on ROCK activity is at least partially mediated by inhibition of the kinase activity of Raf-1.

Taken together, we describe a novel function of BAG1 in neuroregeneration in addition to its known neuroprotective properties. Over-expression of BAG1 *in vivo* resulted in decreased lesion-induced cell loss and increased regeneration. We describe a pathway through which BAG1 can regulate ROCK activity and propose a model of BAG1-mediated axonal regeneration *in vivo* and neurite outgrowth *in vitro* (Fig. 7). Based on our findings, we postulate that BAG1 activates Raf-1, which leads to the activation of the MAPK pathway. Activation of ERK may play a role in enhancement of the intrinsic capability of neurons to

regenerate by stimulating neurite outgrowth, but might not be sufficient by itself to overcome inhibitory signals impeding neurite outgrowth. On the other hand, active Raf-1 physically interacts with and inhibits ROCK activity. Under control conditions, Raf-1 levels do not significantly restrain ROCK activity, leading to limitations in outgrowth and regenerative potential. In contrast, BAG1-over-expression stimulates Raf-1 activation and subsequent ROCK inhibition. This decreased ROCK enzymatic activity, in addition to the translocation of ROCK2 from a membrane-bound to cytosolic and perinuclear space, may result in modulation of actin cytoskeleton and growth cones and thus prevent growth cone collapse through blockade of inhibitory signalling. BAG1 thus simultaneously exerts cytoprotective effects, increases intrinsic axonal regenerative potential and reduces inhibitory axonal signalling via ROCK, making it a promising candidate for future therapeutic approaches targeting CNS regeneration *in vivo*.

References

Bähr M. Live or let die – retinal ganglion cell death and survival during development and in the lesioned adult CNS. Trends Neurosci 2000; 23: 483–490.

Barres BA, Silverstein BE, Corey DP, Chun LL. Immunological, morphological, and electrophysiological variation among retinal ganglion cells purified by panning. Neuron 1988; 1: 791–803.

Bhowmick NA, Ghiassi M, Aakre M, Brown K, Singh V, Moses HL. TGF-beta-induced RhoA and p160ROCK activation is involved in the inhibition of Cdc25A with resultant cell-cycle arrest. Proc Natl Acad Sci USA 2003; 100: 15548–53.

Brennscheidt U, Riedel D, Kolch W, Bonifer R, Brach MA, Ahlers A, et al. Raf-1 is a necessary component of the mitogenic response of the human megakaryoblastic leukemia cell line MO7 to human stem cell factor, granulocyte-macrophage colony-stimulating factor, interleukin 3, and interleukin 9. Cell Growth Differ 1994; 5: 367–72.

Dietz GP, Dietz B, Bahr M. Bcl-x(L) increases axonal numbers but not axonal elongation from rat retinal explants. Brain Res Bull 2006; 70: 117–23.

Ehrenreiter K, Piazzolla D, Velamoor V, Sobczak I, Small JV, Takeda J, et al. Raf-1 regulates Rho signaling and cell migration. J Cell Biol 2005; 168: 955–64.

Gotz R, Wiese S, Takayama S, Camarero GC, Rossoll W, Schweizer U, et al. Bag1 is essential for differentiation and survival of hematopoietic and neuronal cells. Nat Neurosci 2005; 8: 1169–78.

Grimm D, Kern A, Rittner K, Kleinschmidt JA. Novel tools for production and purification of recombinant adenoassociated virus vectors. Hum Gene Ther 1998; 9: 2745–60.

Kermer P, Digicaylioglu MH, Kaul M, Zapata JM, Krajewska M, Stenner-Liewen F, et al. BAG1 over-expression in brain protects against stroke. Brain Pathol 2003; 13: 495–506.

Kermer P, Klöcker N, Labes M, Bähr M. Inhibition of CPP32-like proteases rescues axotomized retinal ganglion cells from secondary cell death in vivo. J Neurosci 1998; 18: 4656–62.

Kermer P, Krajewska M, Zapata JM, Takayama S, Mai J, Krajewski S, et al. Bag1 is a regulator and marker of neuronal differentiation. Cell Death Differ 2002; 9: 405–13.

Kugler S, Lingor P, Scholl U, Zolotukhin S, Bahr M. Differential transgene expression in brain cells in vivo and in vitro from AAV-2 vectors with small transcriptional control units. Virology 2003; 311: 89–95.

Kugler S, Meyn L, Holzmuller H, Gerhardt E, Isenmann S, Schulz JB, et al. Neuron-specific expression of therapeutic proteins: evaluation of different cellular promoters in recombinant adenoviral vectors. Mol Cell Neurosci 2001; 17: 78–96.

Leaver SG, Cui Q, Bernard O, Harvey AR. Cooperative effects of bcl-2 and AAV-mediated expression of CNTF on retinal ganglion cell survival and axonal regeneration in adult transgenic mice. Eur j Neurosci 2006a; 24: 3323–32.

Leaver SG, Cui Q, Plant GW, Arulpragasam A, Hisheh S, Verhaagen J, et al. AAV-mediated expression of CNTF promotes long-term survival and regeneration of adult rat retinal ganglion cells. Gene Ther 2006b; 13: 1328–41.

Liman J, Ganesan S, Dohm CP, Krajewski S, Reed JC, Bahr M, et al. Interaction of BAG1 and Hsp70 mediates neuroprotectivity and increases chaperone activity. Mol Cell Biol 2005; 25: 3715–25.

Lingor P, Koeberle P, Kugler S, Bahr M. Down-regulation of apoptosis mediators by RNAi inhibits axotomy-induced retinal ganglion cell death in vivo. Brain 2005; 128: 550–8.

Lingor P, Teusch N, Schwarz K, Mueller R, Mack H, Bahr M, et al. Inhibition of Rho kinase (ROCK) increases neurite outgrowth on chondroitin sulphate proteoglycan in vitro and axonal regeneration in the adult optic nerve in vivo. J Neurochem 2007; 103: 181–9.

Lingor P, Tonges L, Pieper N, Bermel C, Barski E, Planchamp V, et al. ROCK inhibition and CNTF interact on intrinsic signalling pathways and differentially regulate survival and regeneration in retinal ganglion cells. Brain 2008; 131: 250–63.

Liu L, Hsu SS, Kalia SK, Lozano AM. Injury and strain-dependent dopaminergic neuronal degeneration in the substantia nigra of mice after axotomy or MPTP. Brain Res 2003; 994: 243–52.

Malik JM, Shevtsova Z, Bahr M, Kugler S. Long-term in vivo inhibition of CNS neurodegeneration by Bcl-XL gene transfer. Mol Ther 2005; 11: 373–81.

Markus A, Zhong J, Snider WD. Raf and akt mediate distinct aspects of sensory axon growth. Neuron 2002; 35: 65–76.

Matsui T, Amano M, Yamamoto T, Chihara K, Nakafuku M, Ito M, et al. Rho-associated kinase, a novel serine/threonine kinase, as a putative target for small GTP binding protein Rho. Embo J 1996; 15: 2208–16.

Meberg PJ, Bamburg JR. Increase in neurite outgrowth mediated by overexpression of actin depolymerizing factor. J Neurosci 2000; 20: 2459–69.

Morice C, Nothias F, Konig S, Vernier P, Baccarini M, Vincent JD, et al. Raf-1 and B-Raf proteins have similar regional distributions but differential subcellular localization in adult rat brain. Eur J Neurosci 1999; 11: 1995–2006.

Mueller BK, Mack H, Teusch N. Rho kinase, a promising drug target for neurological disorders. Nat Rev Drug Discov 2005; 4: 387–98.

Olah Z, Komoly S, Nagashima N, Joo F, Rapp UR, Anderson WB. Cerebral ischemia induces transient intracellular redistribution and intranuclear translocation of the raf proto-oncogene product in hippocampal pyramidal cells. Exp Brain Res 1991; 84: 403–10.

Park K, Luo JM, Hisheh S, Harvey AR, Cui Q. Cellular mechanisms associated with spontaneous and ciliary neurotrophic factor-cAMP-induced survival and axonal regeneration of adult retinal ganglion cells. J Neurosci 2004; 24: 10806–15.

Piazzolla D, Meissl K, Kucerova L, Rubiolo C, Baccarini M. Raf-1 sets the threshold of Fas sensitivity by modulating Rok-alpha signaling. J Cell Biol 2005; 171: 1013–22.

Rapp UR, Heidecker G, Huleihel M, Cleveland JL, Choi WC, Pawson T, et al. raf family serine/threonine protein kinases in mitogen signal transduction. Cold Spring Harb Symp Quant Biol 1988; 53 Pt 1: 173–84.

Schwab ME. Nogo and axon regeneration. Curr Opin Neurobiol 2004; 14: 118–24.

Song J, Takeda M, Morimoto RI. Bag1-Hsp70 mediates a physiological stress signalling pathway that regulates Raf-1/ERK and cell growth. Nat Cell Biol 2001; 3: 276–82.

Straten G, Schmeer C, Kretz A, Gerhardt E, Kugler S, Schulz JB, et al. Potential synergistic protection of retinal ganglion cells from axotomy-induced apoptosis by adenoviral administration of glial cell line-derived neurotrophic factor and X-chromosome-linked inhibitor of apoptosis. Neurobiol Dis 2002; 11: 123–33.

Takayama S, Sato T, Krajewski S, Kochel K, Irie S, Millan JA, et al. Cloning and functional analysis of BAG-1: a novel Bcl-2-binding protein with anti-cell death activity. Cell 1995; 80: 279–84.

Takayama S, Xie Z, Reed JC. An evolutionarily conserved family of Hsp70/Hsc70 molecular chaperone regulators. J Biol Chem 1999; 274: 781–6.

Wang HG, Takayama S, Rapp UR, Reed JC. Bcl-2 interacting protein, BAG-1, binds to and activates the kinase Raf-1. Proc Natl Acad Sci USA 1996; 93: 7063–8.

Yoneda A, Multhaupt HA, Couchman JR. The Rho kinases I and II regulate different aspects of myosin II activity. J Cell Biol 2005; 170: 443–53.

Zeiner M, Gehring U. A protein that interacts with members of the nuclear hormone receptor family: identification and cDNA cloning. Proc Natl Acad Sci USA 1995; 92: 11465–9.

Zolotukhin S, Byrne BJ, Mason E, Zolotukhin I, Potter M, Chesnut K, et al. Recombinant adeno-associated virus purification using novel methods improves infectious titer and yield. Gene Ther 1999; 6: 973–85.